View metadata, citation and similar papers at core.ac.uk
brought to you by CORE
provided by Repository@Nottingham

Effect of the substitution position (2, 3 or 8) on the spectroscopic and photophysical properties of BODIPY dyes with a phenyl, styryl or phenylethynyl group

Angel Orte,[†,a] Elke Debroye,[b] María J. Ruedas-Rama,[a] Emilio Garcia-Fernandez,[a] David Robinson,[c] Luis Crovetto,[a] Eva M. Talavera,[a] Jose M. Alvarez-Pez,[a] Volker Leen,[b] Bram Verbelen,[b] Lucas Cunha Dias de Rezende,[b,d] Wim Dehaen,[b] Johan Hofkens,[b] Mark Van der Auweraer[b] and Noël Boens[†,b]

ABSTRACT. A very active branch of organic chemistry is putting great effort in tailoring fluorescent dyes for a myriad of applications, from technological to bioanalytical and biomedical applications. Among the major families of fluorophores, those derived from 4,4-difluoro-4-bora-3a,4a-diaza-*s*-indacene (BODIPY dyes) are undergoing a recent boost thanks to the simplicity and robustness of the chemistry involved. The BODIPY core can be modified with numerous side groups, the 8-position being a modification place with important effects on the spectroscopic and photophysical properties of the resulting dyes. Likewise, previous work has shown that the addition of groups attached at the 3- and 2-positions can result in dyes with very different properties. Herein, we generalize the effect of the substituent side groups by studying nine BODIPY dyes substituted with a phenyl, styryl or phenylethynyl moiety at the 2-, 3- or 8-position of the BODIPY scaffold. Within the class of phenyl- or phenylethynyl-substituted dyes, substitution at the 2-position always leads to dyes with the broadest bandwidths and the largest Stokes shifts. We investigate the solvent effect on the spectroscopic properties of the dyes, using four empirical solvent scales (dipolarity, polarizability, acidity and basicity: Catalán, *J. Phys. Chem*., 2009, **113**, 5951). These analyses identify solvent dipolarity and polarizability as critical parameters accounting for the observed solvent-dependent shifts of the absorption and emission maxima. Finally, time-dependent density functional theory calculations provide insights into the structural and energetic issues concerning the spectroscopic properties of these fluorophores.

KEYWORDS: Fluorescent dyes, solvent effect, Catalán solvent scales, quantum chemical calculations

TOC

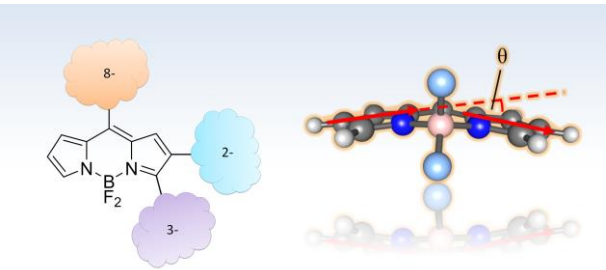

Understanding the spectroscopic properties of BODIPY dyes for a rationale design of tailored fluorescent probes.

a. *Department of Physical Chemistry, Faculty of Pharmacy, University of Granada, Cartuja Campus, 18071 Granada, Spain.*
b. *Department of Chemistry, KU Leuven (Katholieke Universiteit Leuven), Celestijnenlaan 200f, 3001 Leuven, Belgium.*
c. *School of Chemistry, University Of Nottingham, University Park, Nottingham, NG7 2RD, United Kingdom.*
d. *Faculdade de Ciências Farmacêuticas de Ribeirão Preto, Universidade de São Paulo, Av. Do Café s/n, Ribeirão Preto, SP, 14040-903, Brazil.*
† Corresponding authors: AO: E-mail: angelort@ugr.es, tel. +34-958243825. NB, E-mail: Noel.Boens@kuleuven.be
Electronic Supplementary Information (ESI) available: Figures S1-S14, Tables S1-S6, details on the spectral features of **2-Styryl** and **8-Styryl**, and details on the solvatochroism study. See DOI: 10.1039/x0xx00000x

Introduction

The family of 4,4-difluoro-4-bora-3a,4a-diaza-*s*-indacene derivatives, better known as BODIPY (*bo*ron *dipy*rromethene or *bo*ron *dipy*rrin[1-3], Chart 1) dyes, entail a rapidly growing class of compounds, characterized by extremely favorable fluorescent features, such as tunable excitation/emission wavelengths in the visible spectral range, narrow spectral bandwidths and good (photo)chemical stability. Likewise, relatively high molar absorption coefficient, $\varepsilon(\lambda)$, and fluorescence quantum yield, Φ, values lead to a high brightness of these dyes.[4] A very active branch of scientific development is putting great effort in fine-tuning the BODIPY properties by introducing suitable chemical groups onto the central core. As a result, the BODIPY family is expanding constantly and has found applications in wide-ranging fields, from technological (organic light-emitting diodes,[5-7] dye-sensitized solar cells[8-9]) to analytical and *in vivo* imaging applications.[10-11]

Recent advances in organic synthesis have expanded the possibilities of controlled modification of the BODIPY moiety, including substitution by tailored groups at every position of the core.[12] The direct conjugation of fused π-systems, extended π-bonds, the addition of alkyl or aryl groups, or the insertion of electron withdrawing or donating substituents have different effects on the spectroscopic and photophysical properties of the resulting dyes [fluorescence quantum yield (Φ) and lifetime (τ), absorption and emission energies (λ_{abs} and λ_{em}), Stokes shift ($\Delta\bar{\nu}$), full width at half maximum of the absorption and emission band ($fwhm_{abs}$ and $fwhm_{em}$), etc.]. For instance, fusing rigid π-conjugated carbocycles to the BODIPY core results in near-infrared emitting dyes.[13-16]

Modification at the 8- (or *meso*-) position (Chart 1) results in a variety of substituent-promoted effects, as quantum chemical calculations have demonstrated the presence of a node in the HOMO at this position and a significant increase of the electron density upon excitation.[17] Alkylation at the *meso*-position usually has a mild effect, resulting in boron dipyrromethenes with emission maxima around 500 nm and large fluorescence quantum yield values.[17-18] Nevertheless, we recently found that a *tert*-butyl group at the 8- position causes an important decrease in the fluorescence quantum yield Φ and lifetime τ of the resulting dye, as well as a significant red shift of the fluorescence and, consequently, a striking 1560 cm^{-1} Stokes shift $\Delta\bar{\nu}$, much larger than those of other *meso*-alkylated analogues.[19] Boron dipyrromethenes, modified at the *meso*-position with strong electron withdrawing groups, possess large red shifts,[20-21] because the LUMO is highly stabilized[3] compared to unsubstituted BODIPY.[3, 22-24] In contrast, electron donating groups at the *meso*-position cause a blue-shift in the absorption and emission spectra, while keeping high fluorescence quantum yields and lifetimes.[25-28] Certain modifications at the *meso*-position may result in almost nonfluorescent compounds, as for *meso*-alkenyl-[29] or *meso*-formylBODIPYs.[30] Likewise, a *meso*-phenylBODIPY dye is also weakly fluorescent.[31-32] However, *meso*-phenylBODIPYs can display bright fluorescence, depending on the dihedral angle and steric hindrance of the rotation of the phenyl group with respect to the BODIPY core plane. For instance, while phenyl or *p-tert*-butylphenyl substituents at the *meso*-position cause low Φ and τ values, *o*-tolyl- or mesityl groups result in boron dipyrromethene dyes with high Φ (> 0.90).[32] The enhanced nonradiative deactivation in 8-phenyl- or *p-tert*-butylphenyl-substituted BODIPYs is attributed to the population of a distorted conformation of the BODIPY framework in the excited state, leading to loss of planarity.[32] Another example of the effect of the dihedral angle of the *meso*-phenyl substituent on the fluorescence properties of the dyes can be found in the comparison between *meso*-phenyl-3,5-dimethylBODIPY,[33] *meso-p*-methylphenyl-3,5-dimethylBODIPY and *meso-p*-methylphenyl-1,3,5,7-tetramethylBODIPY.[34] While the 3,5-dimethyl substitution gives rise to moderate Φ values (0.17-0.42 for *meso*-phenyl- and 0.11-0.29 for *meso-p*-methylphenyl-substituted boron dipyrromethenes, depending on the solvent), the addition of two methyl groups at the positions 1- and 7- causes an increase in the fluorescence, with Φ up to the range 0.46-0.72.[34]

Although substituents at the 8-position have normally the largest effect on the photophysical properties of BODIPY derivatives, modifications at the 3- and 2-positions also give rise to dyes with diverse properties. Extending the conjugation with double bonds at the 3-position yields fluorophores with a high brightness. However, when the conjugation of the BODIPY framework is extended at the 2-position, dyes with a large Stokes shift $\Delta\bar{\nu}$, but lower Φ value, are obtained. In a preliminary study, our group described this effect for styryl and triazolyl substituents introduced at either the 3- or the 2-position.[35]

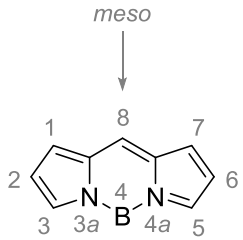

Chart 1. Representation of the "BODIPY core" and its IUPAC numbering system. Common BODIPYs have two fluorine atoms bound to the boron atom (4-position).

In this work, we generalize the effect of the substituent at the 2-, 3- or 8- position of the BODIPY core. Hence, we investigate nine 4,4-difluoro-4-bora-3a,4a-diaza-*s*-indacene dyes substituted with a phenylethynyl or styryl moiety at the 2, 3 or 8-position (**2-Ethyn**, **3-Ethyn**, **8-Ethyn**, **2-Styryl**, **3-Styryl** and **8-Styryl**), a *p-tert*-butylphenyl group at the 2- or 3-position (**2-Ph** and **3-Ph**) and phenyl at the 8-position (**8-Ph**) (Chart 2). The full characterization of the 8-phenylethynyl derivative (**8-Ethyn)** has been reported previously[27] and has been included for discussion purposes. The spectroscopic and photophysical characteristics of these compounds have been investigated in a series of solvents by UV-vis spectrophotometry and steady-state and time-resolved fluorescence spectroscopy. These experiments allow us to determine the relevant spectroscopic and photophysical properties: spectral shape and maxima [λ_{abs}(max) and λ_{em}(max], Stokes shifts ($\Delta\overline{\nu}$), bandwidths ($fwhm_{abs}$ and $fwhm_{em}$), fluorescence quantum yields (Φ), fluorescence lifetimes (τ) and rate constants of fluorescence (k_f) and nonradiative (k_{nr}) deactivation processes. We investigate the solvent effect on the spectroscopic properties of the dyes, according to a generalized procedure based on a set of four empirical solvent scales: dipolarity, polarizability, acidity and basicity of the medium.[36] Time-dependent density functional theory (TD-DFT) calculations provide insights into the structural and energetic properties concerning the spectroscopic parameters of the dyes investigated.

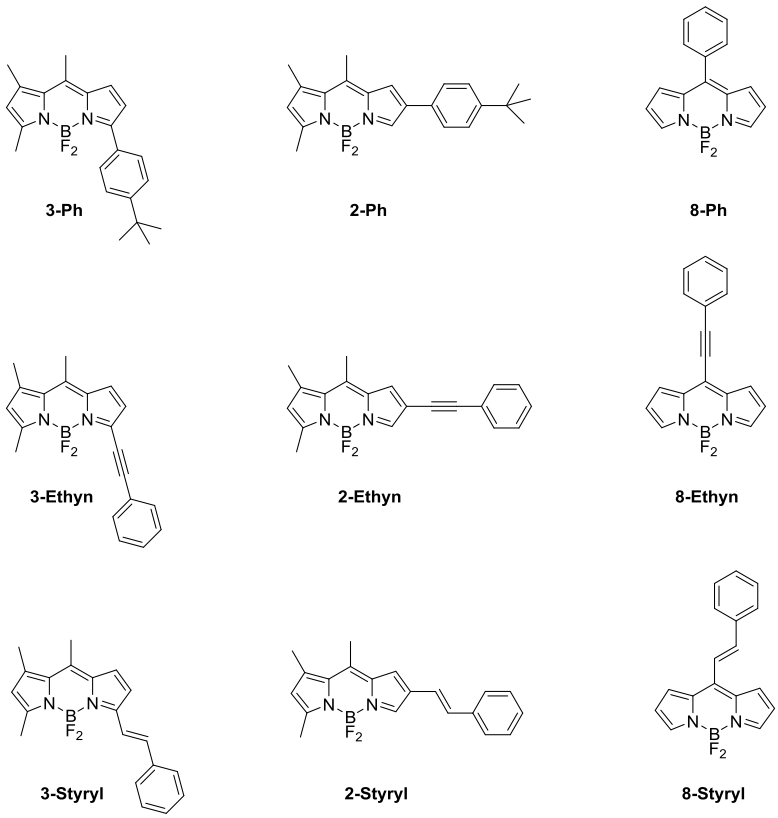

Chart 2. Chemical structures of the BODIPY derivatives studied in this work.

Results and Discussion

Synthesis reactions.

Nine BODIPY derivatives (Chart 2) having three types of substituents, at either the 2-, 3- or 8-position, have been prepared for this study: phenyl derivatives (**2-Ph**, **3-Ph** and **8-Ph**), phenylethynyl derivatives (**2-Ethyn**, **3-Ethyn** and **8-Ethyn**) and styryl derivatives (**2-Styryl**, **3-Styryl** and **8-Styryl**). The synthesis of **2-Ph**, **3-Ph**, **2-Ethyn** and **3-Ethyn** was carried out by following our previously reported procedure,[37] whereas the synthesis of **8-Ph** was performed as described by Kee *et al.*[32] Also **8-Ethyn**[26] and **3-Styryl**[35] were synthesized prepared according to our protocols. Novel synthetic procedures for BODIPY derivatives **2-Styryl** and **8-Styryl** are described next.

2-Styryl [4,4-difluoro-5,7,8-trimethyl-2-(*E*)-styryl-4-bora-3a,4a-diaza-*s*-indacene] was prepared as follows (Scheme 1): To a stirred solution of BODIPY **1** (117 mg, 0.33 mmol, prepared as in reference [37]) in toluene (5 mL) at room temperature, (*E*)-styrylboronic acid (64 mg, 0.43 mmol) and tetrakis(triphenylphosphine) palladium (4 mg, 3.4 µmol) were added, followed by the addition of 1.5 mL of Na_2CO_3 1M (aq). The solution was heated to reflux and after 3 h the reaction mixture was poured in Et_2O (300 mL) and dried over magnesium sulfate. Compound **2-Styryl** (24 mg, 0.072 mmol, 22% yield) was obtained as a dark purple solid powder after purification by silica gel column chromatography [petroleum ether/dichloromethane, 2:1 – 1:1 (v/v)]. M.p. 219 °C. NMR spectra (Figures S1 and S2 in the Electronic Supplementary Information, ESI): ^{1}H NMR (600 MHz, $CDCl_3$) δ 7.77 (s, 1H), 7.45 (d, *J* = 7.4 Hz, 2H), 7.34 (t, *J* = 7.4 Hz, 2H), 7.23 (t, *J* = 7.4 Hz, 1H), 7.16 (s, 1H), 6.98 (d, *J* = 16.3 Hz, 1H), 6.91 (d, *J* = 16.3 Hz, 1H), 6.17 (s, 1H), 2.58 (s, 3H), 2.57 (s, 3H), 2.43 (s, 3H) ppm. ^{13}C NMR (75 MHz, $CDCl_3$) δ 160.5, 145.6, 141.5, 137.7, 137.1, 134.9, 134.6, 129.5, 128.8, 127.6, 127.4, 126.2, 123.1, 120.6, 119.4, 77.2, 17.1, 16.6, 15.1 ppm. LRMS (EI): 336, 316 (M – F).

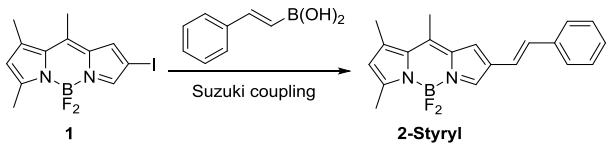

Scheme 1. Schematic representation of the synthesis of **2-Styryl**.

8-Styryl [4,4-difluoro-8-(*E*)-styryl-4-bora-3a,4a-diaza-*s*-indacene] was prepared as follows (Scheme 2): To a solution of BODIPY **2** (310 mg, 1.5 mmol, prepared as in reference [38]) in toluene (15 mL) under continuous stirring at 110 °C, benzaldehyde **3** (200 µL, 1.97 mmol), acetic acid (1.2 mL, 20.9 mmol) and piperidine (1.0 mL, 10.1 mmol) were added. Instantaneous formation of a red-colored compound was observed. After 5 min, the solution was cooled to room temperature and the solvent was evaporated. After silica column purification [petroleum ether/dichloromethane, 1:9 (v/v)], **8-Styryl** (127 mg, 0.43 mmol, 29% yield) was obtained as a dark solid. M.p. 140 °C. NMR spectra (Figures S3 and S4): ^{1}H NMR (600 MHz, $CDCl_3$) δ 7.89 (s, 2H), 7.62 (d, *J* = 6.6 Hz, 2H), 7.52 (d, *J* = 15.9 Hz, 1H), 7.48 – 7.42 (m, 4H), 7.37 (s, 2H), 6.56 (s, 2H) ppm. ^{13}C NMR (75 MHz, $CDCl_3$) δ 144.71, 143.75, 143.02, 135.53, 133.83, 130.54, 129.17, 128.28, 127.98, 121.13, 117.89 ppm. HRMS (EI) calculated for $C_{17}H_{13}BF_2N_2$ 294.1140, found 294.1143. LRMS (EI): 294, 273 [M – F].

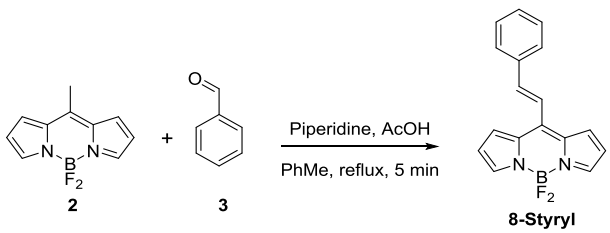

Scheme 2. Schematic representation of the synthesis of **8-Styryl**.

All BODIPY dyes synthesized for this study are solid powders with a strongly colored metallic shine and form intensely colored solutions. When irradiated in solution, a generally bright fluorescence can be observed. In the following sections, we describe the spectroscopic and photophysical features of these dyes, including solvent effects.

Spectroscopic and photophysical properties.

The UV–vis absorption and fluorescence emission spectra of the nine compounds dissolved in 18 solvents (see Table S1 in the ESI) have been measured. The dyes exhibit typical BODIPY-like absorption spectra with a narrow band due to the $S_1 \leftarrow S_0$ transition and a shoulder at lower wavelengths. A blue-shifted, weak $S_2 \leftarrow S_0$ transition band is also detectable in some of the spectra.

Among the phenyl-substituted BODIPY dyes (**2-Ph**, **3-Ph** and **8-Ph**), some differences in absorption behavior are observed. The presence of the *p-tert*-butylphenyl moiety shifts the absorption maximum λ_{abs}(max) from 516–530 nm when this group is at the 2-position (**2-Ph**) to 513–527 nm when it is at the 3-position (**3-Ph**). In both cases, λ_{abs}(max) is more red-shifted in the more polarizable solvents toluene and chlorobenzene. In contrast, the values of λ_{abs}(max) of **8-Ph** (with a phenyl substituent at the *meso*-position) are blue-shifted in relation to those of **2-Ph** and **3-Ph** and are close to those of unsubstituted boron dipyrromethene,[3, 22-24] ranging from 489 nm in acetonitrile to 497 nm in toluene and chlorobenzene: the solvent dependence correlating with the refractive index. This absorption energy range is in good agreement with that of other BODIPYs substituted at the *meso*-position with a weak electron acceptor or donor.[33, 39] One should also note that the absorption spectrum of **8-Ph** is similar to BODIPY dyes substituted by a mesityl or *o*-tolyl moiety in 8-position. This is due to the large dihedral angle (60°) between the BODIPY and phenyl moiety found for **8-Ph** by X-ray diffraction,[32] which reduces the delocalization of the electron cloud of the BODIPY moiety over the phenyl group.[27]

For the phenylethynylBODIPYs (**2-Ethyn**, **3-Ethyn** and **8-Ethyn**), the absorption spectra exhibit also the characteristic features of typical BODIPYs. **2-Ethyn** possesses an absorption maximum between 503 and 525 nm, whereas the λ_{abs}(max) of **3-Ethyn** varies between 525 and 545 nm (Figure 1A). For both dyes, the lowest λ_{abs}(max) value is found in acetonitrile and the largest in cyclohexane. Remarkably, the effect of the substitution position (2 *vs*. 3) on λ_{abs}(max) is much larger for the phenylethynyl moiety than for the phenyl group and, moreover, is opposite: moving the *p-tert*-butylphenyl substituent from the 2- (**2-Ph**) to the 3-position (**3-Ph**) causes a 3 nm blue shift of λ_{abs}(max), whereas the analogous change from **2-Ethyn** to **3-Ethyn** results in a ca. 20 nm red shift of λ_{abs}(max). The previously reported **8-Ethyn**[27] is bathochromically shifted with respect to **2-Ethyn** and **3-Ethyn**, with λ_{abs}(max) ranging from 537 to 547 mm (see Table S2) parallel with an increasing refractive index. As the HOMO of the BODIPY core has a node in the 8-position, these data suggest that the 8-phenylethynyl moiety acts as an electron acceptor stabilizing the LUMO. This rationale also helps to account for the difference between **2-Ethyn** and **3-Ethyn**. The resonance forms of BODIPY suggest that, as in the 8-position, the coefficient of the HOMO in the 3-postion is smaller than in the 2-position, the opposite being the case for those of the LUMO. Hence if the phenylethynyl moiety stabilizes the LUMO rather than destabilizing the HOMO, its effect and hence the red shift *vs*. unsubstituted BODIPY, will be most outspoken for **3-Ethyn** and **8-Ethyn**. Strikingly, the λ_{abs}(max) values of the **8-Ph** are blue shifted with respect to those of **3-Ph** and **2-Ph**.

Styryl-substituted BODIPYs (**2-Styryl**, **3-Styryl** and **8-Styryl**) exhibit different absorption properties. **3-Styryl** displays a main, narrow $S_1 \leftarrow S_0$ transition band (Figure 2A) similar to other 3-substituted boron dipyrromethenes.[35, 37] The λ_{abs}(max) values range from 549 to 561 nm, with a typical red shift from acetonitrile to chlorobenzene. The extended conjugation provided by the styryl functional group causes an extra bathochromic shift of around 20 nm with respect to **3-Ethyn**, and ca. 30 nm with respect to **3-Ph**. In contrast, **2-Styryl** and **8-Styryl** exhibit a clear dual-band absorption and emission behavior (Figures S5). The relative abundance of each band varies with the solvent, and the absorption and the excitation spectra do not match. Multi-exponential fluorescence decay traces were also found for both dyes. Likewise, both BODIPY dyes undergo changes in the relative absorption of each band with time (Figure S6) and completely discolor after 180 min in solvents such as THF and cyclohexanone, even when the solution is kept in the dark. This effect is especially observed for **2-Styryl**, but can also be detected for **8-Styryl**. This is indicative of (photo-)instability of the dyes. Because of this (photo-)instability, no further experiments were performed with **2-Styryl** and **8-Styryl**.

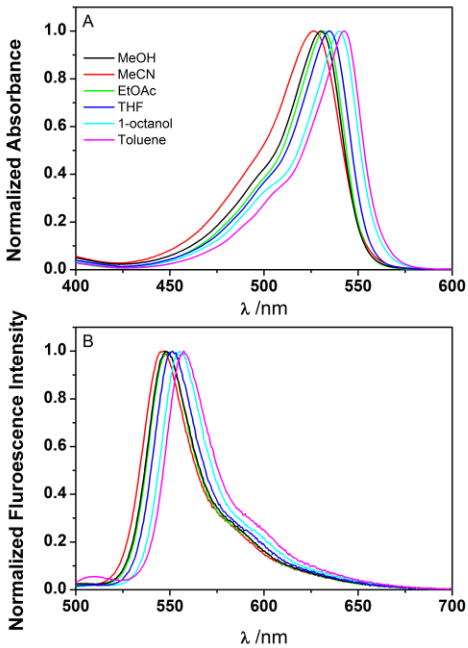

Figure 1. (A) Normalized absorption spectra of **3-Ethyn** in a selection of solvents. (B) Corresponding normalized fluorescence emission spectra upon excitation at 488 nm.

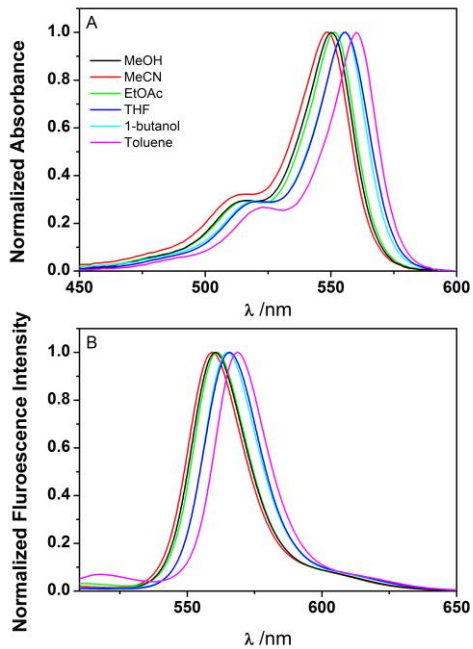

Figure 2. (A) Normalized absorption spectra of **3-Styryl** in a selection of solvents. (B) Corresponding normalized fluorescence emission spectra upon excitation at 510 nm.

The most interesting spectroscopic features are related to the fluorescence emission of the BODIPY derivatives. Herein, we compare the maxima of the emission spectra [λ_{em}(max)], Stokes shifts ($\Delta\,\overline{n}$), fluorescence quantum yields (Φ) and lifetimes (τ), and other fluorescence-related properties of the dyes studied.

A comparison of the phenyl-substituted BODIPY dyes (**2-Ph**, **3-Ph** and **8-Ph**) already highlights very remarkable differences (Tables 1 and 2). **3-Ph** and **8-Ph** display the characteristic emission features of boron dipyrromethenes: (a) a mirror image-shaped, narrow emission band ($fwhm_{em}$ averaged over all the solvents tested equals 1060 ± 50 cm^{-1} and 1390 ± 110 cm^{-1} for **3-Ph** and **8-Ph**, respectively); (b) a small Stokes shift $\Delta\,\overline{n}$ [in

the 859–1111 cm^{-1} range for **3-Ph** (average $\Delta\bar{\nu}$ = 990 ± 67 cm^{-1}) and in the 633–856 cm^{-1} range for **8-Ph** (average $\Delta\bar{\nu}$ = 726 ± 62 cm^{-1})]; (c) emission maxima λ_{em}(max) that are red-shifted in the more polarizable solvents [λ_{em}(max) moves from 544 nm in acetonitrile to 554 nm in chlorobenzene and toluene for **3-Ph**, whereas for **8-Ph** λ_{em}(max) varies from 507 nm in methanol to 517 nm in toluene and 518 nm in cyclohexane]. The $fwhm_{em}$ results are intermediate between those of 8-methylBOBIPY ($fwhm_{em}$ around 950 cm^{-1})[19] and those of *meso*-halogenated BODIPYs ($fwhm_{em}$ around 1400 cm^{-1}), as is the trend in the emission maxima λ_{em}(max) with the different solvents. However, the Stokes shifts $\Delta\bar{\nu}$ are larger than those reported for *meso*-alkylated and *meso*-halogenated BODIPY dyes, which are in the 400 cm^{-1} range.[17, 33, 40] For instance, *meso-p*-methylphenyl-3,5-dimethylBODIPY and *meso-p*-methylphenyl-1,3,5,7-tetramethylBODIPYs exhibit $\Delta\bar{\nu}$ values between 513 and 627 cm^{-1},[34] and between 447 and 560 cm^{-1} for *meso*-phenyl-3,5-dimethylBODIPY.[33] Concerning the solvent dependence of these spectroscopic parameters, one can observe that while for **3-Ph** $\Delta\bar{\nu}$, $fwhm_{abs}$ and $fwhm_{em}$ increase more or less parallel with the dielectric constant ε of the solvent, this relation is quite erratic for $\Delta\bar{\nu}$ and $fwhm_{em}$ of **8-Ph**.

In order to better understand the differences between different of BODIPYs, we also analyzed the relation between $\Delta\bar{\nu}$ and $fwhm_{em}$ or $fwhm_{abs}$ more quantitatively. If only low frequency molecular vibrations ($h\nu_{vib} < kT$) contribute to $\Delta\bar{\nu}$ and $fwhm_{em}$ or $fwhm_{abs}$, the relation between both properties is given by eqn (1):[41-43]

$$(fwhm)^2 = 16 (\ln 2)\, E_R\, kT \qquad (1)$$

where E_R is the excess energy with which a vertical transition from the minimum of the ground state reaches the excited state potential energy surface (PES) upon absorption of a photon (and analogously for emission). Hence the Stokes shift $\Delta\bar{\nu}$ is $2E_R$. For T = 290 K, eqn (1) can be expressed as: $\Delta\bar{\nu} = 8.9514 \times 10^{-4}\,(fwhm)^2$ (in cm^{-1}). For **3-Ph** and **8-Ph** the average $fwhm_{em}$ is respectively 1060 ± 50 cm^{-1} and 1390 ± 110 cm^{-1}, which yields a respective average Stokes shift $\Delta\bar{\nu}$ of 1010 and 1730 cm^{-1} using eqn (1). For **3-Ph** this matches the average experimental $\Delta\bar{\nu}$ value of 990 cm^{-1}. However, for **8-Ph** the average $\Delta\bar{\nu}$ value calculated according to eqn (1) is more than twice as large as the experimental value, which is only 726 cm^{-1}. When instead of the average values of $fwhm_{em}$ the average values of $fwhm_{abs}$ are used, one finds 2320 cm^{-1} and 1030 cm^{-1} for the average calculated $\Delta\bar{\nu}$ of **3-Ph** and **8-Ph**, respectively. Now the average value of the experimental $\Delta\bar{\nu}$ of **3-Ph** is overestimated by more than a factor of 2, whereas the agreement with that of **8-Ph** is marginal. While for **3-Ph** the $fwhm_{abs}$ is significantly broader than $fwhm_{em}$ (1610 *vs*. 1060 cm^{-1}), the reverse trend is observed for **8-Ph** (1080 *vs*. 1390 cm^{-1}). This would suggest that for **3-Ph** the PES is steeper in the excited state than in the ground state, while for **8-Ph** the opposite is suggested. The steep PES for the ground state could be due to steric hindrance. In contrast to what was observed earlier for molecules with a strongly dipolar excited state,[43] the values of the Stokes shift estimated from the $fwhm_{abs}$ and $fwhm_{em}$ are overestimated and the deviation becomes stronger for broader bands. Especially when the bands of the BODIPY derivatives get broader, $fwhm_{abs}$ and $fwhm_{em}$ are no longer uniquely determined by low frequency (torsional) vibrations but also envelope the 0–1 high frequency vibronic band. However, the absorption and emission maxima whose position determines the Stokes shift always corresponds with the 0–0 vibronic band of the high frequency vibration for the compounds studied here. The emission maximum of **2-Ph** varies with the solvent, ranging from 566 nm in cyclohexane to 583 nm in cyclohexanone and acetone. The spectral emission features of **2-Ph** differ significantly from those of **3-Ph** and **8-Ph**. **2-Ph** exhibits a much broader emission band (average $fwhm_{em}$ = 2050 ± 240 cm^{-1}) than **3-Ph** and **8-Ph** do, as well as a larger Stokes shift $\Delta\bar{\nu}$ (average $\Delta\bar{\nu}$ = 1799 ± 243 cm^{-1}). Moreover, $fwhm_{abs}$ of **2-Ph** (2200 ± 50 cm^{-1}) is similar to $fwhm_{em}$ and hence quite broader than the average $fwhm_{abs}$ of **3-Ph** (1610 cm^{-1}) and **8-Ph** (1080 cm^{-1}). As observed for **8-Ph**, the average $\Delta\bar{\nu}$ of **2-Ph**, as calculated from $fwhm_{em}$ using eqn (1), is much larger than the experimental value (3750 cm^{-1} *vs.* 1799 cm^{-1}). When the values of $fwhm_{abs}$ are used to calculate the average Stokes shift of **2-Ph** an even larger value of 4340 cm^{-1} is found. However, in contrast to what was observed for **8-Ph**, but in accordance to what was found for **3-Ph**, $fwhm_{em}$, $fwhm_{abs}$ and $\Delta\bar{\nu}$ of **2-Ph** increase roughly parallel with the dielectric constant ε of the solvent. **3-Ph** exhibits large Φ values, from 0.81 to 1.00, which are in good agreement with previously reported ones,[35, 37] except for **3-Ph** in toluene that shows a slightly larger Φ in this work. Regarding the rate constants of radiative (k_f) and nonradiative (k_{nr}) S_1 deactivation, **3-Ph** shows an increase of k_f with solvent refractive index n, from 1.6×10^8 s^{-1} in methanol to 2.2×10^8 s^{-1} in toluene, whereas k_{nr} ranges from negligible values in diethyl ether and 1,4-dioxane to 0.4×10^8 s^{-1} in methanol. **2-Ph** shows remarkable differences in the Φ values as a function of the solvent used, ranging from 0.359 to 0.72. For **2-Ph**, there is no clear trend in the solvent dependence of k_f with an average value of $(1.0 \pm 0.1) \times 10^8$ s^{-1}. For k_{nr} an increase with the dielectric constant ε of the solvent can be observed. The average k_{nr} value of **2-Ph** amounts to $(0.9 \pm 0.2) \times 10^8$ s^{-1}. The larger values of k_{nr} observed for **2-Ph** compared to **3-Ph**, correlate with its larger values of $fwhm_{em}$ and $\Delta\bar{\nu}$, suggesting a larger displacement of the PES of the ground state and the excited state. This larger displacement leads to a better Franck-Condon factor between the zeroth vibrational level of the excited state and an iso-energetic vibrational level of the ground state.[33] In contrast to **2-Ph** and **3-Ph**, substitution at the *meso*-position in

8-Ph diminishes drastically the Φ values (similar to the values observed earlier in toluene),[32] so that **8-Ph** is a much less bright fluorescent dye than its 2- and 3-phenyl-substituted equivalents. The average k_f value of **8-Ph** is (2.8 ± 0.9) × 10^8 s^{-1}, in the same range as for the 2- and 3-substituted analogues. However, k_{nr} is much larger, with an average value of (33 ± 12) × 10^8 s^{-1}, due to a different equilibrium position along the rotational coordinate in the ground and excited state.[32-33] This makes the fluorescence lifetime τ much shorter for **8-Ph** than for **2-Ph** and **3-Ph** (Fig. S7). For k_f of **8-Ph** there is no trend in the solvent dependence. The highest k_{nr} values of **8-Ph** are found for the highly polar, nonpolarizable solvents methanol, acetonitrile and acetone while the lowest k_{nr} values are observed for the nonpolar, highly polarizable solvents chloroform, toluene and chlorobenzene. There is however no clear relation with solvent polarity of polarizability. A previous publication suggested that this could be due to the effect of the environment viscosity.[32] Tables 1 and 2 compile the spectroscopic and photophysical data of **2-Ph**, **3-Ph** and **8-Ph** as a function of solvent.

Table 1. Spectroscopic and photophysical data of **3-Ph** and **2-Ph** as a function of solvent. The solvents are numbered according to increasing refractive index *n* as in Table S1.

Product		Solvent	λ_{abs} (max) [nm]	λ_{em} (max) [nm]	$\Delta\bar{\eta}$ [cm^{-1}]	$fwhm_{abs}$ [cm^{-1}]	$fwhm_{em}$ [cm^{-1}]	Φ [a]	τ [b] [ns]	k_f [c] [10^8 s^{-1}]	k_{nr} [c] [10^8 s^{-1}]
3-Ph	1	CH_3OH	517	547	1061	1680	1110	0.81 ± 0.01	5.13	1.58 ± 0.02	0.37 ± 0.02
	2	CH_3CN	513	544	1111	1700	1170	0.895 ± 0.001	5.08	1.76 ± 0.01	0.21 ± 0.01
	3	$(C_2H_5)_2O$	522	549	942	1530	1040	1.00 ± 0.02	5.11	1.96 ± 0.04	0.00 ± 0.04
	4	Acetone	518	547	1023	1630	1110	0.895 ± 0.005	5.09	1.76 ± 0.01	0.21 ± 0.01
	5	EtOAc [d]	519	547	986	1630	1090	0.86 ± 0.02	4.89	1.76 ± 0.04	0.29 ± 0.04
	6	2-Propanol	520	550	1049	1620	1080	0.91 ± 0.01	4.96	1.84 ± 0.02	0.18 ± 0.02
	7	PrCN [d]	518	548	1057	1670	1090	0.99 ± 0.03	4.90	2.02 ± 0.06	0.02 ± 0.06
	8	Bu_2O [d]	525	551	899	1520	1010	0.96 ± 0.08	4.84	1.98 ± 0.17	0.08 ± 0.17
	9	THF [d]	522	551	1008	1570	1060	0.877 ± 0.009	4.71	1.86 ± 0.02	0.26 ± 0.02
	10	1-Pentanol	523	552	1005	1600	1040	0.899 ± 0.007	4.81	1.87 ± 0.02	0.21 ± 0.02
	11	1,4-Dioxane	521	550	1012	1650	1060	1.00 ± 0.05	4.65	2.15 ± 0.11	0.00 ± 0.11
	12	CH_2Cl_2	521	551	1045	1660	1100	0.87 ± 0.01	4.99	1.74 ± 0.02	0.26 ± 0.02
	13	c-C_6H_{12} [d]	527	552	859	1470	960	0.99 ± 0.07	4.68	2.12 ± 0.15	0.02 ± 0.15
	14	1-Octanol	525	553	964	1550	1020	0.92 ± 0.04	4.76	1.93 ± 0.08	0.17 ± 0.08
	15	$CHCl_3$	524	553	1001	1630	1050	0.94 ± 0.09	4.99	1.88 ± 0.18	0.12 ± 0.18
	16	c-$C_6H_{10}O$ [d]	522	551	1008	1640	1070	0.99 ± 0.06	4.54	2.18 ± 0.13	0.02 ± 0.13
	17	Toluene	527	554	925	1580	1000	0.97 ± 0.02	4.39	2.21 ± 0.05	0.07 ± 0.05
	18	PhCl [d]	527	554	925	1610	1030	0.94 ± 0.09	4.36	2.16 ± 0.21	0.14 ± 0.21
2-Ph	1	CH_3OH	519	582	2086	2300	2320	0.359 ± 0.005	4.23	0.85 ± 0.01	1.52 ± 0.01
	2	CH_3CN	516	581	2168	2260	2440	0.442 ± 0.005	4.89	0.90 ± 0.01	1.14 ± 0.01
	3	$(C_2H_5)_2O$	525	573	1596	2190	1960	0.58 ± 0.02	5.98	0.97 ± 0.03	0.70 ± 0.03
	4	Acetone	519	583	2115	2270	2310	0.47 ± 0.01	5.11	0.92 ± 0.02	1.04 ± 0.02
	5	EtOAc [d]	521	576	1833	2250	2110	0.56 ± 0.01	5.47	1.02 ± 0.02	0.80 ± 0.02
	6	2-Propanol	522	581	1945	2240	2160	0.61 ± 0.02	5.08	1.20 ± 0.04	0.77 ± 0.04
	7	PrCN [d]	520	582	2049	2230	2280	0.36 ± 0.02	5.18	0.69 ± 0.04	1.24 ± 0.04
	8	Bu_2O [d]	527	571	1462	2160	1770	0.58 ± 0.06	5.87	1.0 ± 0.1	0.7 ± 0.1
	9	THF [d]	525	581	1836	2190	2090	0.571 ± 0.004	5.34	1.07 ± 0.01	0.80 ± 0.01
	10	1-Pentanol	525	580	1806	2180	2050	0.61 ± 0.01	5.24	1.16 ± 0.02	0.74 ± 0.02
	11	1,4-Dioxane	524	575	1693	2140	1990	0.57 ± 0.02	5.76	0.99 ± 0.04	0.75 ± 0.04
	12	CH_2Cl_2	523	581	1909	2160	2150	0.57 ± 0.02	5.53	1.03 ± 0.04	0.78 ± 0.04
	13	c-C_6H_{12} [d]	528	566	1272	2180	1500	0.72 ± 0.05	5.80	1.24 ± 0.09	0.48 ± 0.09
	14	1-Octanol	527	579	1704	2200	2030	0.50 ± 0.02	5.56	0.90 ± 0.04	0.90 ± 0.04
	15	$CHCl_3$	526	582	1829	2140	2000	0.52 ± 0.04	5.75	0.90 ± 0.07	0.83 ± 0.07
	16	c-$C_6H_{10}O$ [d]	523	583	1968	2240	2180	0.43 ± 0.02	5.19	0.83 ± 0.04	1.10 ± 0.04
	17	Toluene	530	575	1477	2110	1800	0.63 ± 0.02	5.50	1.15 ± 0.04	0.67 ± 0.04
	18	PhCl [d]	529	582	1721	2150	1960	0.53 ± 0.06	5.40	1.0 ± 0.1	0.9 ± 0.1

[a] Fluorescence quantum yield ± one standard uncertainty. Φ determined *vs*. rhodamine 6G in water (Φ_r = 0.76) as a reference.

[b] Fluorescence lifetimes obtained with λ_{ex} = 488 nm, and λ_{em} (**3-Ph**) = 560, 565, 570 nm or λ_{em} (**2-Ph**) = 560, 570, 580 nm. The standard errors are obtained from the diagonal elements of the covariance matrix available from the global analysis fit of decay traces recorded at three emission wavelengths λ_{em} and are between 6 and 10 ps for **3-Ph** and between 7 and 17 ps for **2-Ph**

[c] The propagated errors are calculated using the uncertainty (standard deviation) of Φ and the standard error of τ.

[d] EtOAc = ethyl acetate, PrCN = butanenitrile, Bu_2O = dibutyl ether, THF = tetrahydrofuran, c-C_6H_{12} = cyclohexane, c-$C_6H_{10}O$ = cyclohexanone, PhCl = chlorobenzene.

Table 2. Spectroscopic and photophysical data of **8-Ph** as a function of solvent. The solvents are numbered according to increasing refractive index *n*.

Product		Solvent	λ_{abs} (max) [nm]	λ_{em} (max) [nm]	$\Delta\bar{\nu}$ [cm^{-1}]	fwhm$_{abs}$ [cm^{-1}]	fwhm$_{em}$ [cm^{-1}]	Φ [a]	τ [b] [ps]	k_f [c] [10^8 s^{-1}]	k_{nr} [c] [10^8 s^{-1}]
8-Ph	1	CH_3OH	490	507	684	1180	1340	0.044 ± 0.004	189	2.3 ± 0.2	50.6 ± 0.4
	2	CH_3CN	489	510	842	1320	1420	0.041 ± 0.004	181	2.3 ± 0.2	53.0 ± 0.4
	3	$(C_2H_5)_2O$	492	509	679	1000	1240	0.050 ± 0.006	235	2.1 ± 0.3	40.4 ± 0.3
	4	Acetone	491	509	720	1180	1270	0.045 ± 0.006	180	2.5 ± 0.3	53.1 ± 0.5
	5	EtOAc [d]	491	509	720	1090	1460	0.056 ± 0.004	220	2.5 ± 0.2	42.9 ± 0.3
	6	2-Propanol	492	511	756	1040	1340	0.082 ± 0.004	284	2.9 ± 0.1	32.3 ± 0.2
	7	PrCN [d]	491	511	797	1180	1460	0.06 ± 0.02	240	2.5 ± 0.8	39.2 ± 0.9
	8	Bu_2O [d]	494	512	712	950	1440	0.074 ± 0.004	301	2.5 ± 0.1	30.8 ± 0.2
	9	THF [d]	493	511	715	1080	1250	0.065 ± 0.007	250	2.6 ± 0.3	37.4 ± 0.3
	10	1-Pentanol	494	511	673	1040	1430	0.12 ± 0.01	375	3.2 ± 0.3	23.5 ± 0.3
	11	1,4-Dioxane	494	511	673	1040	1360	0.12 ± 0.01	342	3.5 ± 0.3	25.7 ± 0.3
	12	CH_2Cl_2	493	512	753	1260	1230	0.07 ± 0.01	329	2.1 ± 0.3	28.3 ± 0.3
	13	c-C_6H_{12} [d]	496	518	856	860	1570	0.12 ± 0.02	274	4.4 ± 0.7	32.1 ± 0.7
	14	1-Octanol	495	512	671	990	1390	0.24 ± 0.03	430	5.6 ± 0.7	17.7 ± 0.7
	15	$CHCl_3$	495	512	671	1070	1340	0.10 ± 0.01	456	2.2 ± 0.2	19.7 ± 0.2
	16	c-$C_6H_{10}O$ [d]	495	511	633	1030	1390	0.07 ± 0.01	259	2.7 ± 0.4	35.9 ± 0.4
	17	Toluene	497	517	778	980	1570	0.096 ± 0.007	434	2.2 ± 0.2	20.8 ± 0.2
	18	PhCl [d]	497	516	741	1070	1530	0.10 ± 0.01	473	2.1 ± 0.2	19.0 ± 0.2

[a] Fluorescence quantum yield ± one standard uncertainty. Φ determined *vs*. rhodamine 6G in water (Φ_r = 0.76) as a reference.

[b] The standard error on the fluorescence lifetime is 1 ps [obtained from the diagonal elements of the covariance matrix available from the global analysis fit of decay traces recorded at three emission wavelengths λ_{em} (515, 520, 525 nm)]. λ_{ex} = 488 nm.

[c] The propagated errors are calculated using the uncertainty (standard deviation) of Φ and the standard error of τ.

[d] see Table 1.

Fluorescence features similar to those of **2-Ph** and **3-Ph** were found for the corresponding 2- and 3-substituted phenylethynyl BODIPY dyes (**2-Ethyn** and **3-Ethyn**). **3-Ethyn** showed fluorescence properties comparable to those of **3-Ph**, i.e., a narrow emission band (fwhm$_{em}$ = 950 ± 50 cm^{-1}) with λ_{em}(max) in the range from 547 nm (in acetonitrile and acetone) to 557 nm (in toluene and chlorobenzene) and a small Stokes shift ($\Delta\bar{\nu}$ = 552 ± 101 cm^{-1}, averaged over all solvents). In analogy to what is found for **3-Ph**, fwhm$_{abs}$ of **3-Ethyn** (1260 ± 160 cm^{-1}) is significantly larger than fwhm$_{em}$. Using eqn (1) and the average value of fwhm$_{em}$, an average Stokes shift $\Delta\bar{\nu}$ of 800 cm^{-1} is obtained for **3-Ethyn**, which agrees marginally with the experimental average value of $\Delta\bar{\nu}$. However, based on the average value of fwhm$_{abs}$ an average value of $\Delta\bar{\nu}$ of 1430 cm^{-1} is calculated using eqn (1), which is ca. three times larger than the experimental value. Figure 1B shows the fluorescence emission spectra of **3-Ethyn** in a selection of solvents. **3-Ethyn** exhibits large Φ values, from 0.77 (in cyclohexanone) to 1.00 in several solvents, which is in good agreement with previous reports.[35, 37] Likewise, the fluorescence lifetime τ decreases from 5.17 ns in methanol to 4.35 ns in chlorobenzene (Figure S8). These Φ and τ values involve an increase in k_f in more polarizable solvents, ranging from (1.6-1.7) × 10^8 s^{-1} in acetonitrile and methanol to (2.2-2.3) × 10^8 s^{-1} in chlorobenzene and toluene, combined with low values for k_{nr}. As found for **3-Ph**, the higher k_f values of **3-Ethyn** are found for highly polarizable, nonpolar solvents (e.g., toluene and chlorobenzene) whereas polar, nonpolarizable solvents (e.g., methanol and acetonitrile) yield the lowest k_f values. Also in analogy with **3-Ph**, the k_{nr} values of **3-Ethyn** do not show a clear solvent dependence, but they always remain smaller than k_f. **2-Ethyn** displays a fluorescence behavior similar to that of **2-Ph**: a broad emission band (fwhm$_{em}$ = 1960 ± 210 cm^{-1}) with λ_{em}(max) varying between 556 nm (in cyclohexane) and 569 nm (in butanenitrile) and a 3-fold larger Stokes shift

$\Delta\bar{\nu}$ (1720 ± 301 cm^{-1}, averaged over all solvents) than the corresponding **3-Ethyn** ($\Delta\bar{\nu}$ = 552 ± 101 cm^{-1}) and **8-Ethyn** ($\Delta\bar{\nu}$ = 464 ± 33 cm^{-1}). In parallel with what was observed for **2-Ph**, fwhm$_{abs}$ of **2-Ethyn** (2210 ± 110 cm^{-1}) is only slightly larger than fwhm$_{em}$. Using eqn (1) and the average value of fwhm$_{em}$, an average $\Delta\bar{\nu}$ value of 3440 cm^{-1} is calculated for **2-Ethyn**, which is again twice the experimental value. Based on the average value of fwhm$_{abs}$, an average $\Delta\bar{\nu}$ value of 4360 cm^{-1} is found using eqn (1), which is again more than twice the experimental value. The Φ values range from 0.20 (in cyclohexanone) to 0.72 (in toluene). The latter is slightly higher than the previously reported value of 0.61.[35] Our results for Φ of **2-Ethyn** in THF, methanol and acetonitrile are in good agreement with previously reported data.[35] In similarity with **2-Ph**, the fluorescence decay rate constant k_f of **2-Ethyn**, with a similar average value of (1.1 ± 0.3) × 10^8 s^{-1}, does not display any clear solvent dependent trend. The solvent effect on k_{nr} of **2-Ethyn** is similar to that of **2-Ph**. As discussed for **2-Ph**, the larger value of k_{nr} of **2-Ethyn** compared to **3-Ethyn** can be related to the broader absorption and emission bands and the larger Stokes shift. As observed for **2-Ph** and **3-Ph**, the values of k_f of **2-Ethyn** [(1.1 ± 0.3) × 10^8 s^{-1}] amount to about 50 % of those of **3-Ethyn** [(1.9 ± 0.2) × 10^8 s^{-1}]. With these k_f and k_{nr} values, the fluorescence lifetime τ of **2-Ethyn** is in the range from 3.70 to 5.09 ns (Figure S8). Table 3 compiles the spectroscopic and photophysical properties of **2-Ethyn** and **3-Ethyn**. These data confirm the different performance of BODIPY dyes substituted at the 2- and 3-positions. For **8-Ethyn**, the average Stokes shift calculated using eqn (1) with the average value of fwhm$_{em}$, 1390 cm^{-1}, amounts to 1720 cm^{-1}, which is nearly four times the experimental value of 464 cm^{-1}. However, when the average fwhm$_{abs}$ value, 960 cm^{-1}, is used an average value of 820 cm^{-1} is calculated for $\Delta\bar{\nu}$, which is still nearly twice the experimental value. When the phenyl-substituted BODIPYs are compared to their ethynylphenyl-substituted counterparts, the average values of $\Delta\bar{\nu}$, fwhm$_{abs}$ and fwhm$_{em}$ are largest for the 2-substituted BODIPYs. For 3-substituted BODIPYs, fwhm$_{abs}$ is larger than fwhm$_{em}$, which indicates a steeper PES in the excited state compared to the ground state for the rotation of the substituent, while the opposite (i.e., steeper PES in the ground state than in the excited state) occurs for the 8-substituted BODIPYs for which fwhm$_{abs}$ is smaller than fwhm$_{em}$. For the 2-subsituted BODIPYs, fwhm$_{abs}$ and fwhm$_{em}$ are nearly the same, but are much larger than those observed for the 3- and 8-substituted BODIPYs indicating a larger difference in the equilibrium position of the rotation angle of the substituent. The Stokes shifts $\Delta\bar{\nu}$ are the smallest for the 8-substituted analogues and the largest for the 2-substituted ones.

In contrast to **8-Ph**, phenylethynyl substitution at the *meso*-position (**8-Ethyn**) did not result in such a large enhancement of nonradiative deactivation, and **8-Ethyn** exhibited large Φ (0.550–0.715) and τ (6.72–7.60 ns) values (Table S2).[27] In parallel with **3-Ph** and **3-Ethyn**, highly polarizable, nonpolar solvents (e.g., toluene and chlorobenzene) yield higher k_f values of **8-Ethyn** than polar, nonpolarizable solvents do (e.g., methanol and acetonitrile), with polarizability being the major factor determining the magnitude of k_f. The larger values of Φ and smaller values of k_{nr} observed for **8-Ethyn** in contrast to **8-Ph** are caused by the extended conjugation of the π-electrons within the triple bond of the *meso*-substituent. Due to the absence of steric hindrance (in contrast to **8-Ph**) there is no exciton phonon coupling with the rotation of the substituent, which could induce a radiationless decay. The most red-shifted λ_{abs}(max) of **8-Ethyn** in the series of phenylethynyl compounds are in contrast to the most blue-shifted λ_{abs}(max) of **8-Ph** in the series of phenyl-substituted dyes.

Table 3. Spectroscopic and photophysical data of **3-Ethyn** and **2-Ethyn**, as a function of solvent. The solvents are numbered according to increasing refractive index *n*.

Product		Solvent	λ_{abs} (max) [nm]	λ_{em} (max) [nm]	$\Delta\bar{\eta}$ [cm^{-1}]	fwhm$_{abs}$ [cm^{-1}]	fwhm$_{em}$ [cm^{-1}]	Φ [a]	τ [b] [ns]	k_f [c] [10^8 s^{-1}]	k_{nr} [c] [10^8 s^{-1}]
3-Ethyn	1	CH_3OH	530	548	620	1330	990	0.86 ± 0.01	5.17	1.66 ± 0.02	0.27 ± 0.02
	2	CH_3CN	525	547	766	1640	1000	0.83 ± 0.01	5.14	1.61 ± 0.02	0.33 ± 0.02
	3	$(C_2H_5)_2O$	536	551	508	1090	910	0.87 ± 0.03	5.15	1.69 ± 0.06	0.25 ± 0.06
	4	Acetone	529	547	622	1430	1000	0.88 ± 0.01	5.12	1.72 ± 0.02	0.23 ± 0.02
	5	EtOAc [d]	532	548	549	1280	940	0.84 ± 0.01	4.92	1.71 ± 0.02	0.33 ± 0.02
	6	2-Propanol	535	552	576	1230	920	0.845 ± 0.001	4.95	1.71 ± 0.01	0.31 ± 0.01
	7	PrCN [d]	530	549	653	1460	1000	0.91 ± 0.03	4.96	1.83 ± 0.06	0.18 ± 0.06
	8	Bu_2O [d]	540	553	435	1030	860	0.868 ± 0.003	4.87	1.78 ± 0.01	0.27 ± 0.01
	9	THF [d]	534	551	578	1250	960	0.84 ± 0.01	4.76	1.76 ± 0.02	0.34 ± 0.02
	10	1-Pentanol	538	554	537	1220	920	0.86 ± 0.02	4.82	1.78 ± 0.04	0.29 ± 0.04
	11	1,4-Dioxane	535	552	576	1380	990	1.00 ± 0.02	4.65	2.15 ± 0.04	0.00 ± 0.04
	12	CH_2Cl_2	535	554	641	1380	940	0.90 ± 0.01	4.78	1.88 ± 0.02	0.21 ± 0.02
	13	c-C_6H_{12} [d]	545	554	298	1100	870	1.0 ± 0.1	4.70	2.1 ± 0.2	0.0 ± 0.2
	14	1-Octanol	540	555	501	1160	950	0.90 ± 0.04	4.71	1.91 ± 0.09	0.21 ± 0.09
	15	$CHCl_3$	539	554	502	1110	880	0.86 ± 0.02	4.77	1.80 ± 0.04	0.29 ± 0.04
	16	c-$C_6H_{10}O$ [d]	534	552	611	1330	1010	0.77 ± 0.08	4.60	1.7 ± 0.2	0.5 ± 0.2
	17	Toluene	543	557	463	1110	940	1.00 ± 0.05	4.43	2.3 ± 0.1	0.0 ± 0.1
	18	PhCl [d]	542	557	497	1220	960	0.95 ± 0.09	4.35	2.2 ± 0.2	0.1 ± 0.2
2-Ethyn	1	CH_3OH	509	566	1979	2270	2210	0.38 ± 0.02	3.70	1.03 ± 0.05	1.68 ± 0.05
	2	CH_3CN	503	567	2244	2520	2320	0.337 ± 0.004	4.05	0.83 ± 0.01	1.64 ± 0.01
	3	$(C_2H_5)_2O$	516	560	1523	2160	1880	0.59 ± 0.03	5.09	1.16 ± 0.06	0.81 ± 0.06
	4	Acetone	506	565	2064	2200	2190	0.47 ± 0.02	4.32	1.09 ± 0.05	1.23 ± 0.05
	5	EtOAc [d]	509	562	1853	2220	2020	0.547 ± 0.004	4.63	1.18 ± 0.01	0.98 ± 0.01
	6	2-Propanol	513	566	1825	2260	2030	0.55 ± 0.03	4.36	1.26 ± 0.07	1.03 ± 0.07
	7	PrCN [d]	507	569	2149	2270	2190	0.24 ± 0.01	4.27	0.56 ± 0.02	1.78 ± 0.02
	8	Bu_2O [d]	521	559	1305	2080	1710	0.61 ± 0.05	4.93	1.2 ± 0.1	0.8 ± 0.1
	9	THF [d]	513	562	1700	2190	1980	0.588 ± 0.001	4.58	1.28 ± 0.01	0.90 ± 0.01
	10	1-Pentanol	516	565	1681	2240	1970	0.55 ± 0.03	4.47	1.23 ± 0.07	1.01 ± 0.07
	11	1,4-Dioxane	513	559	1604	2140	1880	0.65 ± 0.02	4.83	1.35 ± 0.04	0.72 ± 0.04
	12	CH_2Cl_2	513	566	1825	2220	2070	0.55 ± 0.02	4.54	1.21 ± 0.04	0.99 ± 0.05
	13	c-C_6H_{12} [d]	525	556	1062	2110	1450	0.71 ± 0.04	4.92	1.44 ± 0.08	0.59 ± 0.08
	14	1-Octanol	517	565	1643	2270	1920	0.56 ± 0.04	4.69	1.19 ± 0.09	0.94 ± 0.09
	15	$CHCl_3$	517	565	1643	2270	1730	0.45 ± 0.04	4.74	0.95 ± 0.08	1.16 ± 0.09
	16	c-$C_6H_{10}O$ [d]	511	567	1933	2160	2100	0.20 ± 0.03	4.34	0.46 ± 0.07	1.84 ± 0.07
	17	Toluene	521	562	1400	2040	1750	0.72 ± 0.02	4.68	1.54 ± 0.04	0.60 ± 0.04
	18	PhCl [d]	520	565	1532	2090	1880	0.61 ± 0.06	4.55	1.3 ± 0.1	0.9 ± 0.1

[a] Fluorescence quantum yield ± one standard uncertainty. Φ determined *vs*. rhodamine 6G in water (Φ_r = 0.76) as a reference.

[b] Fluorescence lifetime. The standard errors are obtained from the diagonal elements of the covariance matrix available from the global analysis fit of decay traces recorded at three emission wavelengths λ_{em} and are between 11 and 14 ps for **3-Ethyn** and between 11 and 14 ps for **2-Ethyn**. For both **3-Ethyn** and **2-Ethyn**: λ_{ex} = 488 nm, and λ_{em} = 560, 563, 566 nm.

[c] The propagated errors are calculated using the uncertainty (standard deviation) of Φ and the standard error of τ.

[d] See Table 1.

Finally, **3-Styryl** – substituted at the 3-position with the (*E*)-styryl group – also shows fluorescence emission spectral features in line with the other 3-substituted dyes. **3-Styryl** reveals a narrow $S_0 \leftarrow S_1$ emission band (fwhm$_{em}$ = 740 ± 30 cm^{-1}), mirror image of the absorption band with λ_{em}(max) undergoing a bathochromic shift from 559 nm in acetonitrile to 570 nm in chlorobenzene. The styryl substituent at the 3-position causes an additional red shift in the absorption spectra compared to **3-Ph** and **3-Ethyn**. However, this effect is less present in the emission spectra, leading to very small Stokes shift values ($\Delta\bar{\eta}$= 297 ± 30 cm^{-1}, averaged over all the solvents). The average $\Delta\bar{\eta}$ values calculated from the average value of fwhm$_{em}$ (740 cm^{-1}) using eqn (1) amounts to 480 cm^{-1} which is close to the average experimental value 297 cm^{-1}. Using the average value of fwhm$_{abs}$ (800

cm^{-1}) the value of 570 cm^{-1} is obtained for $\Delta\bar{\nu}$. When compared to the other 3-substituted derivatives, the phenyl substitution in **3-Ph** is causing the largest Stokes shifts ($\Delta\bar{\nu}$ = 990 ± 67 cm^{-1}), followed by **3-Ethyn** ($\Delta\bar{\nu}$ = 552 ± 101 cm^{-1}) and finally **3-Styryl** ($\Delta\bar{\nu}$= 297 ± 30 cm^{-1}). The different conjugation of the substituents investigated at the 3-position can be rationalized since phenyl substitution creates the largest relaxation of the excited state, whereas styryl substitution produces further stabilization of the ground state. Figure 2B shows selected examples of **3-Styryl** emission spectra. The Φ and τ values for **3-Styryl** decline in more polarizable solvents: Φ decreases from 0.66 in acetonitrile to 0.42 in cyclohexanone, whereas τ changes from 4.66 ns in diethyl ether to 3.89 ns in chlorobenzene. These results can be rationalized as the value of k_f remains largely invariable in the different solvents [average k_f = (1.3 ± 0.1) × 10^8 s^{-1}], whereas k_{nr} of **3-Styryl** increases in more polarizable solvents (from 0.75 × 10^8 s^{-1} in acetonitrile to 1.26 × 10^8 s^{-1} in chlorobenzene). The Φ values reported herein are slightly lower than previously published values in methanol, acetonitrile, THF and toluene;[35] however, our results are self consistent between many other different solvents. The spectroscopic properties of **3-Styryl** are presented in Table 4. As mentioned above, **2-Styryl** and **8-Styryl** are unstable compounds, exhibiting time-dependent, dual-band emission features (see ESI and Figures S5 and S6 for more details).

Table 4. Spectroscopic and photophysical data of **3-Styryl** as a function of solvent. The solvents are numbered according to increasing refractive index *n*.

Product		Solvent	λ_{abs}(max) [nm]	λ_{em}(max) [nm]	$\Delta\bar{\nu}$ [cm^{-1}]	fwhm$_{abs}$ [cm^{-1}]	fwhm$_{em}$ [cm^{-1}]	Φ [a]	τ [b] [ns]	k_f [c] [10^8 s^{-1}]	k_{nr} [c] [10^8 s^{-1}]
3-Styryl	1	CH_3OH	550	560	325	860	760	0.60 ± 0.02	4.62	1.30 ± 0.04	0.87 ± 0.04
	2	CH_3CN	549	559	326	890	780	0.66 ± 0.02	4.54	1.45± 0.04	0.75 ± 0.05
	3	$(C_2H_5)_2O$	553	561	258	760	730	0.58 ± 0.01	4.66	1.24 ± 0.02	0.90 ±0.02
	4	Acetone	550	560	325	860	770	0.60 ± 0.02	4.40	1.36 ± 0.05	0.91 ± 0.05
	5	EtOAc [d]	551	561	324	830	750	0.61 ± 0.02	4.53	1.35 ± 0.04	0.86 ± 0.05
	6	2-Propanol	554	563	289	820	750	0.57 ± 0.01	4.42	1.29 ± 0.02	0.97 ± 0.02
	7	Bu_2O [d]	556	564	255	750	710	0.48 ± 0.03	4.56	1.05 ± 0.07	1.14 ± 0.07
	8	1-Butanol	555	565	319	820	740	0.59 ± 0.04	4.38	1.35 ± 0.09	0.94 ±0.09
	9	THF [d]	556	566	318	840	770	0.55 ± 0.01	4.22	1.30 ± 0.02	1.07 ± 0.03
	10	1-Pentanol	556	566	318	810	750	0.48 ± 0.01	4.30	1.12 ± 0.02	1.21 ±0.03
	11	1,4-Dioxane	555	564	288	800	740	0.56 ± 0.02	4.26	1.31 ± 0.05	1.03 ± 0.05
	12	CH_2Cl_2	556	565	286	820	720	0.59 ± 0.02	4.29	1.38 ± 0.05	0.96 ±0.05
	13	c-C_6H_{12} [d]	558	565	222	660	650	0.53 ± 0.01	4.32	1.23 ± 0.02	1.09 ± 0.03
	14	$CHCl_3$	559	569	314	780	730	0.53 ± 0.08	4.24	1.3 ± 0.2	1.1 ± 0.2
	15	c-$C_6H_{10}O$ [d]	555	565	319	790	750	0.42 ± 0.02	4.08	1.03 ± 0.05	1.42 ± 0.05
	16	Toluene	560	569	282	760	710	0.52 ± 0.02	3.93	1.32 ± 0.05	1.22 ± 0.05
	17	PhCl [d]	561	570	281	770	720	0.51 ± 0.01	3.89	1.31 ± 0.03	1.26 ± 0.03

[a] Fluorescence quantum yield ± one standard uncertainty. Φ determined *vs*. rhodamine 6G in water (Φ_r = 0.76) as a reference.

[b] Fluorescence lifetime. The standard errors are obtained from the diagonal elements of the covariance matrix available from the global analysis fit of decay traces recorded at three emission wavelengths λ_{em} (560, 565 and 570 nm) and are between 12 and 16 ps. λ_{ex} = 532 nm.

[c] The propagated errors are calculated using the uncertainty (standard deviation) of Φ and the standard error of τ.

[d] See Table 1.

Solvatochroism.

It is useful to determine the origin of the solvent-dependent spectral changes by applying the most recent, comprehensive treatment of the solvent effect (based on a set of four empirical, complementary, mutually independent solvent scales, i.e., dipolarity, polarizability, acidity and basicity of the medium) described by Catalán.[36] In this method, the polarizability and dipolarity of a particular solvent are characterized by the parameters SP and SdP, respectively, whereas solvent acidity and basicity are described by the scales SA and SB, respectively. The {SA, SB, SP, SdP} values for a large number of solvents can be found in the literature.[36] Mathematically, the solvent effect on the physicochemical observable *y* can be expressed by the multilinear eqn (2):

$$y = y_0 + a_{SA}\,SA + b_{SB}\,SB + c_{SP}\,SP + d_{SdP}\,SdP \qquad (2)$$

where y_0 denotes the physicochemical property of interest in the gas phase; a_{SA}, b_{SB}, c_{SP} and d_{SdP} are regression coefficients that describe the sensitivity of the property y to the various solvent–solute interaction mechanisms; and {SA, SB, SP, SdP} are independent solvent parameters (indices) accounting for the various types of solvent–solute interactions.

The spectroscopic observables y analyzed in this paper are the absorption maxima $\bar{\nu}_{abs}$ [= $1/\lambda_{abs}$(max)] and the fluorescence emission maxima $\bar{\nu}_{em}$ [= $1/\lambda_{em}$(max)], both expressed in cm^{-1}. The results of the fits of $y = \bar{\nu}_{abs}$ and $y = \bar{\nu}_{em}$ according to eqn (2) are compiled in Table S3 for **3-Ethyn**, **2-Ethyn** and **8-Ethyn**, Table S4 for **3-Ph**, **2-Ph** and **8-Ph**, and Table S5 for **3-Styryl**. Making use of the Catalán solvent scales {SA, SB, SP, SdP} [eqn (2)] gives excellent fits of $y = \bar{\nu}_{abs}$ of **3-Ph**, **2-Ph**, **8-Ph, 3-Ethyn**, **2-Ethyn**, **8-Ethyn** and **3-Styryl** for the solvents listed in the respective Tables (1-4 and S2), using the correlation coefficient r as goodness-of-fit criterion [$r \geq 0.928$, Tables S3-S5, ESI]. Similar high-quality fits were obtained for the multilinear analysis of $y = \bar{\nu}_{em}$ according to eqn (2) ($r \geq 0.844$, Tables S3-S5, ESI).

The unique, extra benefit of the generalized (i.e. Catalán) treatment of the solvent effect is that it allows one to separate the relative contributions of dipolarity, polarizability, acidity and basicity of the medium. Therefore, we utilized the new methodology to resolve which solvent properties are primarily responsible for the observed shifts of $\bar{\nu}_{abs}$ and $\bar{\nu}_{em}$. The relative importance of each of the {SA, SB, SP, SdP} solvent scales was studied by omitting in turn one or two solvent scales from the regression analysis [eqn (2)]. These analyses (Tables S3–S5, ESI) clearly identify solvent dipolarity and polarizability as critical parameters accounting for the experimental solvatochromic shifts of $\bar{\nu}_{abs}$ and $\bar{\nu}_{em}$ of **3-Ethyn**, **2-Ethyn**, **8-Ethyn**, **3-Ph**, **2-Ph**, **8-Ph** and **3-Styryl** (see ESI for details).

Some general trends in the results of the Catalán analyses can be observed. For the absorption spectra ($\bar{\nu}_{abs}$) of all the compounds, d_{SdP} is positive and ranges from 200 to 700, while c_{SP} has much larger, negative values ranging between ca. –1100 and –1450. This indicates that the major effect of the solvent on the absorption spectra is related to the polarizability: an increasing solvent polarizability induces a red shift of λ_{abs}(max). For the emission spectra ($\bar{\nu}_{em}$) of the 3- and 8-substituted BODIPYs, the solvent dependence resembles that of the absorption spectra: c_{SP} is negative with values between –670 and –1570, while d_{SdP} is positive, but with smaller values ranging from 130 to 710. For these dyes, the effect of solvent polarity on λ_{em}(max) is the same as for λ_{abs}(max): a higher polarizability induces a red shift of λ_{em}(max). The situation for the emission spectra of the 2-substituted BODPYs **2-Ph** and **2-Ethyn** is different: negative values are recovered for both c_{SP} and d_{SdP}. How λ_{em}(max) of these dyes moves as a function of the solvent used depends on the relative weights of solvent polarizability (c_{SP}) and dipolar polarity (d_{SdP}). The seemingly erratic dependence of λ_{em}(max) of **2-Ph** and **2-Ethyn** as a function of solvent refractive index n (Table S1) can be rationalized by the substantial influence of solvent dipolarity (ε). The correlation of λ_{em}(max) of **2-Ph** or **2-Ethyn** with solvent polarizability is less obvious as compared to that of the corresponding λ_{abs}(max). The negative c_{SP} and d_{SdP} produce, besides a red shift of λ_{em}(max) with increasing n (polarizability), also a red shift with increasing ε (dipolarity).

Since the first report on the use of the solvent scales {SA, SB, SP, SdP},[36] the physicochemical observables y in eqn (2) have been almost exclusively the spectroscopic parameters $\bar{\nu}_{abs}$ and $\bar{\nu}_{em}$. A plausible reason may be that the accurate determination of the absorption [λ_{abs}(max) = $1/\bar{\nu}_{abs}$] and emission [λ_{em}(max) = $1/\bar{\nu}_{em}$] maxima is straightforward when a wavelength-calibrated spectrophotometer and a wavelength-calibrated, fully corrected – both for the excitation and emission channel – spectrofluorometer are utilized. In principle, however, any solvent-influenced, physicochemical observable can be analyzed using the Catalán approach to determine which solvent property is primarily responsible for its experimental, solvent-dependent behavior. As an example, Figure S10 in the ESI shows that solvent dipolarity, SdP, is an important factor in the variation of $fwhm_{abs}$ and $fwhm_{em}$. In a pioneering paper, we analyzed the solvent-dependent behavior of the kinetic parameters k_f and k_{nr} of three boron dipyrromethene dyes.[44] Since k_f (= Φ/τ) and k_{nr} [$(1 - \Phi)/\tau$] are calculated from the values of fluorescence quantum yield (Φ) and lifetime (τ), obtaining accurate values of k_f and k_{nr} depends critically on the accuracy with which Φ and τ are measured. These measurements are generally more challenging than those of $\bar{\nu}_{abs}$ and $\bar{\nu}_{em}$. One can expect a higher degree of uncertainty of the k_f and k_{nr} values, even when the measurements of Φ and τ have been carefully executed by skilled researchers.

The analyses of the k_f values of **2-Ph**, **2-Ethyn**, **8-Ph** and **3-Styryl** using {SA, SB, SP, SdP} [eqn (2)], and as a function of ε [eqn (3)] and $f(n^2)$ [eqn (4)] indicate that there is no clear trend in the dependence of k_f on solvent (di)polarity (or ε) or polarizability (or n) for these compounds. Conversely, analyses of $y = k_f$ of **3-Ph**, **3-Ethyn** and **8-Ethyn** according to eqn (2) recover positive c_{SP} and significantly (4–5-fold) smaller, negative d_{SdP} estimated values (Table S6). Hence, higher polarizability leads to higher k_f values whereas higher polarity yields lower k_f values. This is in agreement with the observation that the higher k_f values of these dyes are found for highly polarizable, nonpolar solvents (e.g., toluene and chlorobenzene) whereas polar, nonpolarizable solvents (e.g., methanol and acetonitrile) yield the lowest k_f values. Extra linear fits of $y = k_f$ as a function of ε [(di)polarity, eqn

(3)] and as a function of $f(n^2)$ [polarizability, eqn(4)] corroborate that polarizability (n) is more effective than polarity (ε) in influencing the value of k_f (Table S6).

$$y = y_0 + a\,\varepsilon \qquad (3)$$

$$y = y_0 + b\,f(n^2) \text{ with } f(n^2) = (n^2 - 1)/(2n^2 + 1) \qquad (4)$$

Analyses of k_{nr} of **3-Ph** and **3-Ethyn** as a function of {SA, SB, SP, SdP} [eqn (2)], ε [eqn (3)] and $f(n^2)$ [eqn (4)] do not show any clear solvent dependence. The solvent effect on k_f, k_{nr}, λ_{abs}(max) and λ_{em}(max) of **3-Ph** is in complete agreement with that of **3-Ethyn**. Fitting the k_{nr} values of **8-Ethyn** according to eqn (2) gives a good fit with positive, nearly equal c_{SP} and d_{SdP} estimates (Table S6), indicating that polarity and polarizability have equal importance in influencing the value of k_{nr}. The multilinear fit of $y = k_{nr}$ of **2-Ph** according to eqn (2) recovers a small, negative c_{SP} and a 3-fold larger positive d_{SdP} value (Table S6), accounting for the large k_{nr} (> 10^8 s^{-1}) values in the more polar solvents (methanol, acetonitrile, acetone, 2-propanol, butanenitrile and cyclohexanone) with ε > 18 (Table 1). That solvent dielectric constant ε is more crucial than solvent refractive index n in affecting the k_{nr} values of these dyes is corroborated by the significantly superior fit of $y = k_{nr}$ as a function of ε [eqn (3)] compared to that as a function $f(n^2)$ [eqn (4)] (Table S6). Very similar results are obtained for **2-Ethyn** (Table S6). The solvent effect on k_f, k_{nr}, λ_{abs}(max) and λ_{em}(max) of **2-Ph** is completely similar to that of **2-Ethyn**. An excellent multilinear fit of $y = k_{nr}$ of **8-Ph** according to eqn (2) was found with a positive d_{SdP} estimate and a ca. 8-fold higher, negative c_{SP} estimate (Table S6). Higher polarity thus leads to higher k_{nr} values whereas higher polarizability yields lower k_{nr} values. These results are in agreement with the higher k_{nr} values of **8-Ph** obtained in highly polar, nonpolarizable solvents (e.g., methanol, acetonitrile, acetone) compared to those in nonpolar, highly polarizable solvents (e.g., chloroform, toluene, chlorobenzene). That solvent polarizability decreases the k_{nr} values more than that solvent polarity increases them (i.e., polarizability has a higher weight than polarity) is confirmed by the better linear fit of $y = k_{nr}$ as a function of $f(n^2)$ [eqn (4)] than as a function of ε [eqn (3)] (Table S6). Finally, the satisfactory fit of $y = k_{nr}$ of **3-Styryl** according to eqn (2) yields a positive c_{SP} estimate and a ca. 10-fold smaller, negative d_{SdP} value (Table S6), accounting for the highest k_{nr} values observed for the most polarizable, nonpolar solvents. That polarizability is the key factor influencing the k_{nr} values of **3-Styryl** is confirmed by the satisfactory linear fit of $y = k_{nr}$ as a function of $f(n^2)$ [eqn (4)] compared to the unacceptable linear fit *vs*. ε [eqn (3)].

For a visual inspection of the general influence of ε and $f(n^2)$ on the k_f, k_{nr}, λ_{abs}(max) and λ_{em}(max) values for all the studied derivatives, correlation plots have been included in Figures S11-S14 (ESI).

Quantum Chemical Calculations.

Computational approaches have been proven useful in determining the excited-state properties of BODIPY dyes. In a previous study, we demonstrated that the BODIPY core is nonplanar at the relaxed S_1 geometry.[45] We have also demonstrated that bulky substituents at the 8-position on the BODIPY ring lead to very distorted, nonplanar geometries in the S_1 state, leading to a fast nonradiative decay *via* a conical intersection.[19] Lindsey, Holten and coworkers employed the SAC-CI method to investigate phenyl substituents at the 8-position.[32] They found that in the S_1 state, rotation around the bond connecting the phenyl group to the BODIPY ring was barrierless, allowing an efficient coupling to a radiationless deexcitation mechanism, giving rise to the low fluorescence quantum yields observed experimentally. Mukherjee and Thilagar investigated substitutions around the BODIPY core with respect to relative stability of the electronic ground states.[46] They found that alkyl substitutions at the 3/5-positions contributed to a stabilization of the ground-state energy coupled with planar relaxed S_0 geometries.

Given in Table 5 are the angles between the pyrrole rings describing the planarity of the BODIPY core (Figure 3). All of the substituted boron dipyrromethenes considered follow the same trend of becoming less planar in the S_1 state compared to S_0, with five of the nine BODIPY derivatives having an angle greater than 10° at the S_1 relaxed geometry. **8-Styryl** shows significant distortion in the ground state but particularly in the S_1 excited state, with an angle of 40°. By comparison to *meso-tert*-butylBODIPY,[19] we can predict that **8-Styryl** will deexcite *via* radiationless decay.

Table 5. Angle between the planes of the pyrrole rings of the BODIPY core at the S_0 and S_1 relaxed geometries, calculated using ωB97X/6-311G(d).

BODIPY molecule	S_0	S_1
2-Ph	0°	4°
3-Ph	9°	14°
8-Ph	7°	11°
2-Ethyn	0°	2°
3-Ethyn	0°	9°
8-Ethyn	6°	11°
2-Styryl	5°	11°
3-Styryl	4°	7°
8-Styryl	14°	40°

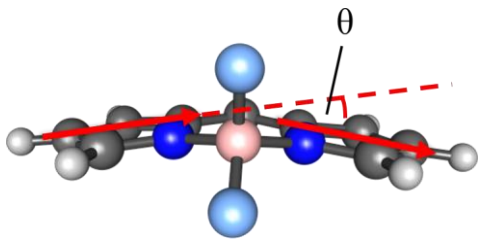

Figure 3. Schematic diagram of the planarity of the BODIPY core, defined as planar when the angle, θ, is equal to zero.

Simulated emission spectra calculated from *ab initio* molecular dynamics (AIMD) are given in Figure 4. The styryl substituted BODIPYs show large shifts in their calculated emission maxima, with **8-Styryl** showing a large shift and a very broad peak. It is worth noting that the calculated emission profiles (and therefore the broadening) are based on the assumption of a normalized emission intensity (i.e., we assume $\Phi = 1$ for each given geometry). Given the nonradiative relaxation mechanism expected for **8-Styryl**, we would expect the calculated profile to be somewhat different to that given in Figure 3, although we cannot calculate the fluorescence quantum yield directly. For the phenyl-substituted dyes the experimentally observed effect of the substitution position on the emission maximum (Tables 1 and 2) agrees well with the simulated emission spectra. Phenyl substitution at the 8-position (**8-Ph**) exhibits the shortest emission maximum, whereas the longest emission maximum corresponds to the **3-Ph**. However, for the phenylethynyl-substituted BODIPYs, the effect of the substitution position is inverted in the simulated spectra when compared to the experimentally obtained spectra. Whereas **2-Ethyn** was found to exhibit the shortest emission maximum in the simulation, the experimental spectra showed that this is the compound with the reddest emission among the phenylethynyl-substituted dyes (Table 3). On the other hand, **3-Ethyn**, the BODIPY with the shortest emission maximum in the experimental spectra (Table 3) shows the largest red shift in the simulation. Furthermore, while for the phenyl-substituted dyes the range of the emission maxima in the simulation is about 50 nm, corresponding to what was found experimentally, this range is for the ethynylphenyl substituted BODIPYs much larger in the simulation (110 nm) than found experimentally (5 nm in toluene).

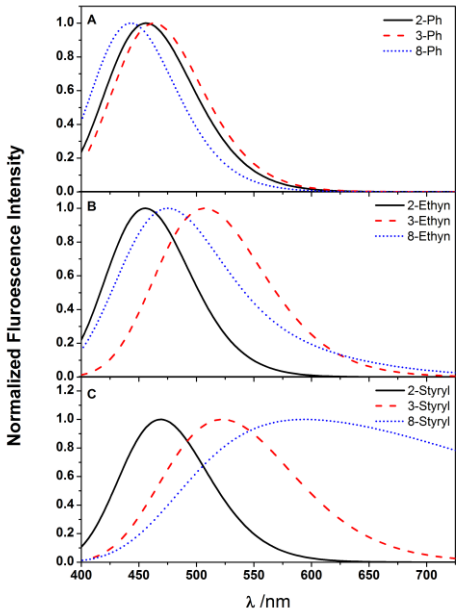

Figure 4. Simulated emission spectra calculated from AIMD trajectories with ωB97X/6-311G(d) of (A) phenyl-, (B) phenylethynyl-, and (C) styrylBODIPYs, substituted at the positions 2 (solid lines), 3 (dashed lines), and 8 (dotted lines).

Besides the emission spectra the calculations also yield information on the dipole moments of the different species involved: relaxed ground state, Franck Condon S_1 excited state, relaxed S_1 excited state, Franck Condon ground state (Table 6). In all cases, except for **2-Styryl,** the relaxed S_0 dipole moment is higher than the relaxed S_1 dipole moment calculated using DFT. For all compounds studied we observe upon excitation, which occurs at the equilibrium geometry of the S_0 state, a decrease of the permanent dipole moment. This explains the positive values obtained for d_{SdP} for $\bar{n}_{abs}$ of all compounds. For all compounds studied we observe upon emission, which occurs at the equilibrium geometry of the S_1 state, an increase of the permanent dipole moment. This explains the positive values obtained for d_{SdP} recovered for $\bar{n}_{em}$ of the 3- and 8-substituted BODIPYs. The increase of the dipole moment upon emission is however in contradiction with the negative values obtained for d_{SdP} for **2-Ph** and **2-Ethyn**. In absorption, the spectral shift of $\bar{n}_{abs}$ is proportional with $\mu_0(\mu_0-\mu_E)$, all dipole moments at the S_0 equilibrium (relaxed) geometry. Conversely, for emission the spectral shift of $\bar{n}_{em}$ is proportional with $\mu_E(\mu_0-\mu_E)$, all dipole moments at the S_1 equilibrium (relaxed) geometry.[47-49] In spite of these predictions we could not find any quantitative correlation between d_{SdP} and either $\mu_0(\mu_0-\mu_E)$ or $\mu_E(\mu_0-\mu_E)$.

While solvent polarity is important, there are some interesting features that cannot be assigned to the dielectric constant ε alone. **3-Ph**, for example, displays a fluorescence quantum yield in acetone of 0.895, while in butanenitrile Φ increases to 0.99, despite ε being approximately equal for the two solvents (20.7 for acetone and 20.3 for butanenitrile). **2-Ethyn** exhibits a Φ value of 0.47 in acetone, and only 0.24 in butanenitrile. In Table 6 the calculated dipole moments of the BODIPY derivatives are given, along with those for acetone and butanenitrile. In all cases, the relaxed S_0 dipole moment is higher than the relaxed S_1 dipole moment using DFT, except for **2-Styryl**. For almost all of the cases observed, high Φ values are seen when the relaxed S_1 dipole moment is lower than the dipole moment of the solvent, with the exception of **3-Ph**. We speculate that where the relaxed S_1 dipole moment is close to (or less than) the dipole moment of the solvent, the conical intersection can be stabilized and hence Φ becomes significantly less than 1. Inspection of the experimental data above confirms that these BODIPY derivatives do indeed show a very solvent dependent behavior with respect to the fluorescence quantum yield.

Table 6. Dipole moments, in Debye, calculated using ωB97X/6-311G(d). The second column refers to the ground-state relaxed dipole moment, while the fifth column refers to the excited-state relaxed dipole moment. The third column refers to the excited-state dipole moment calculated at the relaxed ground-state geometry, while the fourth column refers to the ground-state dipole moment calculated at the relaxed excited-state geometry.

	S_0 Equilibrium (relaxed) Geometry		S_1 Equilibrium (relaxed) Geometry	
BODIPY molecule	S_0 dipole moment	S_1 dipole moment	S_0 dipole moment	S_1 dipole moment
2-Ph	4.92	3.67	4.94	3.84
3-Ph	4.04	2.13	4.27	2.64
8-Ph	5.72	3.53	5.94	3.44
2-Styryl	5.13	4.02	5.51	5.32
3-Styryl	4.05	2.45	4.06	2.71
8-Styryl	6.57	2.97	8.47	3.61
2-Ethyn	5.34	3.35	5.55	4.69
3-Ethyn	4.28	2.08	4.45	1.82
8-Ethyn	6.98	3.03	7.42	2.93

Conclusions

In this work, we have synthesized and characterized, by UV-vis spectrophotometry and steady-state and time-resolved fluorescence spectroscopy, nine BODIPY derivatives substituted with a phenyl, styryl or phenylethynyl group at the 2-, 3- or 8-position, in a large number of solvents. Our data confirm that 3-substitution is beneficial for producing boron dipyrromethenes with sharp absorption bands and high fluorescence quantum yields. All three 3-substituted derivatives (**3-Ph**, **3-Ethyn** and **3-Styryl**) showed these highly favorable features. Conversely, substitution at the 2-position yields BODIPY dyes with large Stokes shifts and broad bands, as found in **2-Ph** and **2-Ethyn**. Substitution at the *meso*-position produces dyes with features similar to the 3-substituted ones, except for *meso*-phenylBODIPY **8-Ph**. Spectroscopically, the behavior of both **3-Ph** and **8-Ph** was in general very similar. However, **8-Ph** exhibited less red-shifted emission bands and, importantly, phenyl-substitution at the *meso*-position remarkably decreased both the quantum yield and fluorescence lifetime through the enhancement of the nonradiative deactivation processes.

Experimental

Instrumentation.

Absorption spectra were collected using a Perkin-Elmer Lambda 650 UV/Vis spectrophotometer. Spectrally corrected steady-state fluorescence emission spectra were collected on a JASCO FP-6500 or an Edinburgh Instruments FL 980 spectrofluorometer. All absorption and fluorescence emission measurements were carried out using undegassed samples in 5×10 mm cuvettes (with 10 mm optical path length for absorption and a 90° angle setup for fluorescence collection through the shortest side), in a Peltier temperature-controlled cell holder set at 20 °C. Fluorescence quantum yield (Φ_x) determination was performed according to eqn (5):[50-51]

$$\Phi_x = \Phi_r \times \frac{F_x}{F_r} \times \frac{1-10^{-A_r(\lambda_{ex})}}{1-10^{-A_x(\lambda_{ex})}} \times \frac{n_x^2}{n_r^2} \qquad (5)$$

where *x* and *r* refer respectively to sample *x* (i.e., BODIPY derivatives) and reference (standard) fluorophore *r* with known quantum yield Φ_r; *F* denotes the integrated fluorescence spectra, with spectral and inner-filter correction (the latter was minimized by keeping the absorbance below 0.1, but in cases of small Stokes shift, the correction was needed); $A(\lambda_{ex})$ stands for the absorbance at the corresponding excitation wavelength; and *n* is the refractive index of the solvent. Rhodamine 6G dissolved in water was employed as the fluorescence quantum yield reference (Φ_r = 0.76).[52] For each quantum yield determination, eight independent Φ_x measurements were performed, using (2 conc. of sample *x*) × (2 conc. of reference *r*) × (2 excitation wavelengths λ_{ex})

Fluorescence lifetimes, τ, were obtained from a χ^2-minimization by iterative reconvolution fitting of the convolution of the δ-response function with the instrumental response function to fluorescence decay traces, recorded using a FluoTime200 fluorometer (PicoQuant GmbH) working in single photon timing mode.[53-55] The pulsed excitation source was either a 485 nm or a 532 nm diode laser (LDH series from PicoQuant GmbH),

operated with a PDL-800 driver (PicoQuant) at a pulse repetition rate of 20 MHz, except for **8-Ph**, whose decay traces were collected at a 40 MHz repetition rate. For each compound in a given solvent, three different fluorescence decay traces were collected at different emission wavelengths, selected by a grating monochromator, after a polarizer set at the 'magic angle'. The fluorescence decay traces were collected over 1320 channels, with a time increment of 36 ps or 18 ps per channel (for 20 MHz or 40 MHz repetition rates, respectively), until they reached 2×10^4 counts in the peak channel. Histograms of the instrument response functions were collected using a LUDOX scatterer.

Quantum chemical calculations.

Structures of the ground (S_0) and the first singlet excited (S_1) state were optimized using unrestricted DFT with the ωB97X functional and the 6-311G(d) basis set. In order to study the first singlet excited state within Kohn-Sham DFT, the maximum overlap method (MOM) was employed to converge the self-consistent field (SCF) procedure to an excited-state solution. In this procedure, an initial set of orbitals for the ground state is generated, then a β electron is excited from the HOMO to the LUMO; the MOM procedure then prevents the variational collapse to the ground state within the subsequent SCF calculation. This approach has the advantage that the orbitals are specifically optimized for the state of interest and the transition energies can be calculated using a ΔSCF approach. This approach is accurate for a large number of states; however, the excitation energy to valence orbitals (i.e. non-Rydberg) leading to open-shell singlet states is usually underestimated. The reason for this deficiency is associated with the use of a single determinant describing a mixed-spin state. The computed excitation energies (and thus gradients) can be improved significantly by applying the Ziegler post-SCF spin-purification correction, eqn (6):

$$E = 2\,E_S - E_T \qquad (6)$$

where E is the energy of the spin-purified (true) singlet state, E_S is the energy of the spin-mixed state and E_T is the energy of the corresponding triplet state. This approach has been successfully applied previously to the BODIPY core.[19, 45] Solvation was taken into account using the polarizable continuum model (PCM), with a dielectric constant set to 37.5 (acetonitrile).

Ab initio molecular dynamics (AIMD) simulations were performed in both the gas phase and solvated phase, using the PCM. All AIMD simulations were run for a total of 10^4 steps, with a time step of 10 a.u. Fock matrix extrapolation was employed, using the last 10 Fock matrices and extrapolated using a 5th-order polynomial. Ground-state and excited-state potential energy surfaces were explored using the MOM method outlined above. All DFT calculations were performed with the Q-Chem software.

Acknowledgments

We acknowledge financial support from the Fonds voor Wetenschappelijk Onderzoek (FWO, grant G.0962.13) and a postdoctoral fellowship to E. D. The authors also thank Belspo for funding through IAP VII-05.

Author contributions

NB, MVdA, JH, WD and AO designed research; ED, VL, BV, LCDdR and WD synthesized the compounds; AO, ED, MJRR, EGF, LC, EMT and JMAP performed the spectroscopic measurements; NB and MVdA performed the solvatochroism study; DR performed the quantum chemical calculations; AO and NB wrote the draft manuscript; all authors reviewed and edited the final version.

References

1. R. P. Haugland, *The Molecular Probes® Handbook—A Guide to Fluorescent Probes and Labeling Technologies*, 11th edn., Life Technologies Corp. , Eugene OR (USA), 2010.
2. G. Ulrich, R. Ziessel and A. Harriman, *Angew. Chem. Int. Ed.*, 2008, **47**, 1184-1201.
3. A. Loudet and K. Burgess, *Chem. Rev.*, 2007, **107**, 4891-4932.

4. S. E. Braslavsky, *Pure Appl. Chem.*, 2007, **79**, 293-465.
5. L. Bonardi, H. Kanaan, F. Camerel, P. Jolinat, P. Retailleau and R. Ziessel, *Adv. Funct. Mater.*, 2008, **18**, 401-413.
6. R. Ziessel, L. Bonardi, P. Retailleau and F. Camerel, *C. R. Chim.*, 2008, **11**, 716-733.
7. N. J. Findlay, J. Bruckbauer, A. R. Inigo, B. Breig, S. Arumugam, D. J. Wallis, R. W. Martin and P. J. Skabara, *Adv. Mater.*, 2014, **26**, 7290-7294.
8. M. Benstead, G. H. Mehl and R. W. Boyle, *Tetrahedron*, 2011, **67**, 3573-3601.
9. S. P. Singh and T. Gayathri, *Eur. J. Org. Chem.*, 2014, **2014**, 4689-4707.
10. N. Boens, V. Leen and W. Dehaen, *Chem. Soc. Rev.*, 2012, **41**, 1130-1172.
11. T. Kowada, H. Maeda and K. Kikuchi, *Chem. Soc. Rev.*, 2015, **44**, 4953-4972.
12. N. Boens, B. Verbelen and W. Dehaen, *Eur. J. Org. Chem.*, 2015, **2015**, 6577-6595.
13. A. B. Descalzo, H.-J. Xu, Z.-L. Xue, K. Hoffmann, Z. Shen, M. G. Weller, X.-Z. You and K. Rurack, *Org. Lett.*, 2008, **10**, 1581-1584.
14. L. Zeng, C. Jiao, X. Huang, K.-W. Huang, W.-S. Chin and J. Wu, *Org. Lett.*, 2011, **13**, 6026-6029.
15. D.-J. Kang, D.-H. Eom, J.-T. Mo, H.-S. Kim, P. Sokkalingam, C.-H. Lee and P.-H. Lee, *Bull. Korean Chem. Soc.*, 2010, **31**, 507-510.
16. S. Yamazawa, M. Nakashima, Y. Suda, R. Nishiyabu and Y. Kubo, *J. Org. Chem.*, 2016, **81**, 1310-1315.
17. J. Bañuelos, I. J. Arroyo-Córdoba, I. Valois-Escamilla, A. Alvarez-Hernández, E. Peña-Cabrera, R. Hu, B. Z. Tang, I. Esnal, V. Martínez and I. López Arbeloa, *RSC Adv.*, 2011, **1**, 677-684.
18. J. Bañuelos-Prieto, A. R. Agarrabeitia, I. Garcia-Moreno, I. Lopez-Arbeloa, A. Costela, L. Infantes, M. E. Perez-Ojeda, M. Palacios-Cuesta and M. J. Ortiz, *Chem. Eur. J.*, 2010, **16**, 14094-14105.
19. L. Jiao, C. Yu, J. Wang, E. A. Briggs, N. A. Besley, D. Robinson, M. J. Ruedas-Rama, A. Orte, L. Crovetto, E. M. Talavera, J. M. Alvarez-Pez, M. Van der Auweraer and N. Boens, *RSC Adv.*, 2015, **5**, 89375-89388.
20. G. Sathyamoorthi, J. H. Boyer, T. H. Allik and S. Chandra, *Heteroatom Chem.*, 1994, **5**, 403-407.
21. S. Choi, J. Bouffard and Y. Kim, *Chem. Sci.*, 2014, **5**, 751-755.
22. A. Schmitt, B. Hinkeldey, M. Wild and G. Jung, *J. Fluoresc.*, 2009, **19**, 755-758.
23. I. J. Arroyo, R. Hu, G. Merino, B. Z. Tang and E. Peña-Cabrera, *J. Org. Chem.*, 2009, **74**, 5719-5722.
24. B. R. Groves, S. M. Crawford, T. Lundrigan, C. F. Matta, S. Sowlati-Hashjin and A. Thompson, *Chem. Commun.*, 2013, **49**, 816-818.
25. C. A. Osorio-Martínez, A. Urías-Benavides, C. F. A. Gómez-Durán, J. Bañuelos, I. Esnal, I. López Arbeloa and E. Peña-Cabrera, *J. Org. Chem.*, 2012, **77**, 5434-5438.
26. V. Leen, P. Yuan, L. Wang, N. Boens and W. Dehaen, *Org. Lett.*, 2012, **14**, 6150-6153.
27. N. Boens, L. Wang, V. Leen, P. Yuan, B. Verbelen, W. Dehaen, M. Van der Auweraer, W. D. De Borggraeve, L. Van Meervelt, J. Jacobs, D. Beljonne, C. Tonnelé, R. Lazzaroni, M. J. Ruedas-Rama, A. Orte, L. Crovetto, E. M. Talavera and J. M. Alvarez-Pez, *J. Phys. Chem. A*, 2014, **118**, 1576-1594.
28. B. Dhokale, T. Jadhav, S. M. Mobin and R. Misra, *Dalton Trans.*, 2015, **44**, 15803-15812.
29. B. Dhokale, T. Jadhav, S. M. Mobin and R. Misra, *Chem. Commun.*, 2014, **50**, 9119-9121.
30. K. Krumova and G. Cosa, *J. Am. Chem. Soc.*, 2010, **132**, 17560-17569.
31. C. Yu, L. Jiao, H. Yin, J. Zhou, W. Pang, Y. Wu, Z. Wang, G. Yang and E. Hao, *Eur. J. Org. Chem.*, 2011, **2011**, 5460-5468.
32. H. L. Kee, C. Kirmaier, L. Yu, P. Thamyongkit, W. J. Youngblood, M. E. Calder, L. Ramos, B. C. Noll, D. F. Bocian, W. R. Scheidt, R. R. Birge, J. S. Lindsey and D. Holten, *J. Phys. Chem. B*, 2005, **109**, 20433-20443.
33. W. Qin, M. Baruah, M. Van der Auweraer, F. C. De Schryver and N. Boens, *J. Phys. Chem. A*, 2005, **109**, 7371-7384.
34. Y. Chen, L. Wan, D. Zhang, Y. Bian and J. Jiang, *Photochem. Photobiol. Sci.*, 2011, **10**, 1030-1038.
35. V. Leen, T. Leemans, N. Boens and W. Dehaen, *Eur. J. Org. Chem.*, 2011, **2011**, 4386-4396.
36. J. Catalán, *J. Phys. Chem. B*, 2009, **113**, 5951-5960.
37. V. Leen, E. Braeken, K. Luckermans, C. Jackers, M. Van der Auweraer, N. Boens and W. Dehaen, *Chem. Commun.*, 2009, 4515-4517.
38. D.-C. Wang, H.-P. Wang, S. Gao, T.-Y. Zhang and X.-J. Peng, *Acta Cryst.*, 2007, **E63**, 2238-2239.
39. W. Qin, M. Baruah, A. Stefan, M. Van der Auweraer and N. Boens, *ChemPhysChem*, 2005, **6**, 2343-2351.
40. E. Palao, A. R. Agarrabeitia, J. Bañuelos-Prieto, T. A. Lopez, I. Lopez-Arbeloa, D. Armesto and M. J. Ortiz, *Org. Lett.*, 2013, **15**, 4454-4457.
41. R. A. Marcus, *J. Chem. Phys.*, 1965, **43**, 1261-1274.
42. B. S. Brunschwig, S. Ehrenson and N. Sutin, *J. Phys. Chem.*, 1987, **91**, 4714-4723.
43. G. Verbeek, S. Depaemelaere, M. Van der Auweraer, F. C. De Schryver, A. Vaes, D. Terrell and S. De Meutter, *Chem. Phys.*, 1993, **176**, 195-213.

44. A. Filarowski, M. Kluba, K. Cieślik-Boczula, A. Koll, A. Kochel, L. Pandey, W. M. De Borggraeve, M. Van der Auweraer, J. Catalán and N. Boens, *Photochem. Photobiol. Sci.*, 2010, **9**, 996-1008.
45. E. A. Briggs, N. A. Besley and D. Robinson, *J. Phys. Chem. A*, 2013, **117**, 2644-2650.
46. S. Mukherjee and P. Thilagar, *RSC Adv.*, 2015, **5**, 2706-2714.
47. V. E. Lippert, *Z. Naturforschg.*, 1955, **10a**, 541-545.
48. N. Mataga, Y. Kaifu and M. Koizumi, *Bull. Chem. Soc. Jpn.*, 1955, **28**, 690-691.
49. N. Mataga, Y. Kaifu and M. Koizumi, *Bull. Chem. Soc. Jpn.*, 1956, **29**, 465-470.
50. B. Valeur and M. N. Berberan-Santos, *Molecular Fluorescence. Principles and Applications.* , 2nd edn. edn., Wiley-VCH Verlag GmbH, Weinheim (Germany), 2012.
51. J. R. Lakowicz, *Principles of Fluorescence Spectroscopy*, 3rd edn., Springer, 2006.
52. J. Olmsted, *J. Phys. Chem.*, 1979, **83**, 2581-2584.
53. H. Lemmetyinen, N. V. Tkachenko, B. Valeur, J.-i. Hotta, M. Ameloot, N. P. Ernsting, T. Gustavsson and N. Boens, *Pure Appl. Chem.*, 2014, **86**, 1969-1998.
54. M. vandeVen, M. Ameloot, B. Valeur and N. Boens, *J. Fluoresc.*, 2005, **15**, 377-413.
55. W. Becker, *Advanced Time-Correlated Single Photon Counting Techniques*, Springer, Berlin (Germany), 2005.